High resolution numerical modelling of flow-vegetation interactions

TIMOTHY I. MARJORIBANKS (IAHR Member), Postdoctoral Research Associate, *Department of Geography, Durham University, Lower Mountjoy, South Road, Durham. DH1 3LE, UK*

Email: tim.marjoribanks@durham.ac.uk (author for correspondence)

RICHARD J. HARDY (IAHR Member), Reader, *Department of Geography, Durham University, Lower Mountjoy, South Road, Durham. DH1 3LE, UK*

Email: r.j.hardy@durham.ac.uk

STUART N. LANE, Professor, *Institute of Earth Surface Dynamics, Faculté des géosciences et de l'environnement, Université de Lausanne, CH-1015 Lausanne, Switzerland*

Email: stuart.lane@unil.ch

DANIEL R. PARSONS, Professor, *Department of Geography, Environment and Earth Sciences, University of Hull, Hull, HU6 7RX, UK*

Email: d.parsons@hull.ac.uk

Running Head: High resolution modelling of flow-vegetation interactions

High resolution numerical modelling of flow-vegetation interactions

ABSTRACT

In this paper we present and apply a new three dimensional model for the prediction of canopy flow and turbulence dynamics in open channel flow. The approach uses a dynamic immersed boundary technique that is coupled in a sequentially staggered manner to a Large Eddy Simulation. Two different biomechanical models are developed depending on whether the vegetation is dominated by bending or tensile forces. For bending plants, a model structured on the Euler-Bernoulli beam equation has been developed, while for tensile plants, an N-pendula model has been developed. Validation against flume data shows good agreement and demonstrates that for a given stem density, the models are able to simulate the extraction of energy from the mean flow at the stem-scale which leads to the drag discontinuity and associated mixing layer.

Keywords: Biomechanics; Large Eddy Simulations; streams and rivers; vegetated flows; vortex dynamics.

1 Introduction

Vegetation within lowland river channels has a profound influence on the functioning of the fluvial system. Historically, vegetation has been seen as problematic due to the reduction in conveyance it can cause through increasing flow resistance (Kadlec 1990, Nepf *et al.* 2007). Thus, the removal of vegetation has been undertaken to accelerate the passage of flow and reduce flood risk (Nepf *et al.* 2007). However, vegetation can also have a positive impact on the river system through promoting sedimentation and nutrient retention (Sand-Jensen *et al.* 1989, López and García 1998, Sand-Jensen 1998), providing stable habitats for terrestrial and aquatic wildlife (Kemp *et al.* 2000, Lopez and Garcia 2001, Liu and Shen 2008, Liu *et al.* 2008) and improving water quality (Schulz *et al.* 2003). Thus, aquatic vegetation can have both beneficial and detrimental effects (Haslam *et al.* 1975) and exhibits a complex relationship with the river system (Nepf 2012, Gurnell 2014).

This paper recognises that management schemes need to be based upon a clear process understanding of the effects of different vegetation species on the flow. It necessitates coupling the plant stem-scale, which drives local energy losses, to the reach-scale, where the integration of these energy losses determines conveyance (Naden *et al.* 2006, Nepf and Ghisalberti 2008). Previous research to understand the interaction between flow and aquatic vegetation canopies (e.g. Ghisalberti and Nepf 2002, Nepf and Ghisalberti 2008) has built upon process understanding gained from terrestrial environments (e.g. Raupach *et al.* 1996, Finnigan 2000). Most of this research has been conducted by applying physically scaled flume experiments (Ghisalberti and Nepf 2002, Wilson *et al.* 2003, Nepf and Ghisalberti

2008). These studies have led to a good process understanding of the mean and turbulent flow associated with canopies: vegetation extracts energy from the flow, via the process of drag, which transfers energy from the mean flow to both heat and to stem-scale turbulence (Yagci and Kabdasli 2008, Zong and Nepf 2010). It has been shown that within canopy flows the drag discontinuity induced by the vegetation creates an inflection point within the mean velocity profile at or close to the canopy top (Nepf 2012). This inflection point leads to the development of Kelvin-Helmholtz instabilities and the generation of coherent roller vortices along the canopy top (Ikeda and Kanazawa 1996, Nezu and Sanjou 2008). However, much of this research has been conducted with rigid (e.g. Dunn *et al.* 1996, Nepf 1999, Liu *et al.* 2008), or idealised vegetation (e.g. Jarvela 2002, Yagci and Kabdasli 2008) that represents a significant simplification of the natural aquatic vegetation most common in lowland rivers (macrophytes). Therefore, further work is required to better understand the effect of complex aquatic vegetation on channel hydraulics (Kemp *et al.* 2000).

Recently, flume (e.g. Siniscalchi and Nikora 2012) and field (e.g. Sukhodolov and Sukhodolova 2010, Sukhodolova and Sukhodolov 2012) studies using natural macrophytes have supported and added to results obtained from flows around idealised macrophytes. For example, Sukhodolov and Sukhodolova (2012) conducted in-depth field analysis of dynamical turbulence characteristics, introducing a phenomenological model for predicting canopy-layer vortex frequency. However, the extent of spatially concurrent flow measurements over a significant spatial area is often limited and analysis of the flow data is commonly restricted to time averaged, bulk hydraulic characteristics which have low temporal and spatial resolution. These data do not always capture the localised turbulent energy dynamics of the plant-flow interaction throughout the canopy.

This paper focuses upon the development of numerical modelling approaches as an alternative to improve our process understanding of turbulence generated from macrophytes. The approach provides a time dependent, high resolution, spatially distributed set of hydraulic data, and as it is grounded in numerical simulation, it can provide the framework for evaluating turbulence, vegetation energy loss relationships, and potentially a step change in our understanding of flow vegetation interaction. Furthermore the models provide an environment within which to analyse particular processes without the data being confounded by the presence of information relating to other, un-modelled processes (Lane *et al.* 1999) and permits a sensitivity analysis of different vegetation configurations and flow conditions.

2 Previous numerical models of flow-vegetation interaction in the fluvial environment

A number of numerical models have previously been developed in order to represent flows

through vegetation. One of the most widely used approaches involves a canopy-scale momentum sink term, based upon the drag force exerted by the vegetation (Fischer-Antze *et al.* 2001, Defina and Bixio 2005). This method requires prior knowledge of properties such as canopy density, projected plant area and a drag coefficient and is therefore not suitable for investigating canopy-flow dynamics as it requires *a priori* assumptions regarding their nature. Such techniques are not suitable for investigating stem-scale turbulent energy dynamics.

To investigate the effect of turbulence production at the wake and leaf scales on turbulence structure and momentum transport, vegetation elements must be modelled at a scale where the vegetation diameter exceeds the spatial grid resolution of the model. This constraint on model resolution has meant that to date, most stem-scale models have focussed on high resolution analysis of smaller-scale canopy properties and have not fully considered large or highly submerged canopies. Stoesser *et al.* (2006) performed Large Eddy Simulation (LES) experiments on an array of submerged cylinders using a spatially variable very fine grid resolution in order to fully capture the stem-scale turbulence. Their results agreed well with previous experimental results, as well as replicating the classical vortex regimes known to be present (e.g. horseshoe, von Karman, rib and roller vortices as well as trailing vortices from the vegetation tops). Subsequent work has developed this analysis and begun to use larger domains, enabling larger patch-scale analysis at stem-scale resolution. Stoesser *et al.* (2010) undertook LES experiments on a patch of emergent vegetation using a combination of high resolution Cartesian and curvilinear grids. They used a range of different vegetation densities and were able to investigate the structural changes to wake turbulence patterns caused by changes in vegetation density and found that these changes had a significant effect on turbulence statistics and flow resistance.

While these stem scale models are capable of capturing the fine turbulence structure with great accuracy, they do not include any treatment of flexible vegetation. Submerged vegetation exhibits four different motion characteristics when exposed to a flow: (i) erect with no movement; (ii) gently swaying; (iii) strong, coherent swaying; and (iv) prone (Nepf and Vivoni 2000). Rigid models are therefore unable to capture the complex feedbacks between flow and vegetation, which influence canopy processes (Nepf and Ghisalberti 2008, Okamoto and Nezu 2009). The first study to include flexible stems was conducted by Ikeda *et al.* (2001). They developed a biomechanical plant model for semi-rigid vegetation such as grasses and reeds (e.g. *Phragmites australis*) within a two dimensional LES framework. However, as the model was only two-dimensional, it was not capable of capturing the full three-dimensional stem-scale energy dynamics. Li and Xie (2011) extended this modelling approach to account for highly flexible vegetation, however the spatial resolution of the model was sufficiently low that stems were not explicitly resolved and thus the model relied upon *a priori* assumptions regarding plant-flow interaction.

Abdelrhman (2007) developed a model for highly flexible stems, based on an N-pendula model to represent plant motion (see Section 3.4). However, this model had several limitations. Notably, it used a simplified flow model which calculated the velocity at different heights based upon known velocity profiles. Therefore, energy loss from the flow was represented by introducing a simple force balance into the flow equation, similar to that used to drive the plant model. The model was therefore able to replicate the familiar mean velocity profile, but could not predict turbulent properties of the flow with accuracy. This approach was further extended by Dijkstra and Uittenbogaard (2010) who included a parameterisation of rigidity within the plant equations, allowing the model to be used more widely for plants exhibiting a range of flexibilities. The model was also used in conjunction within a one-dimensional Reynolds-Averaged Navier-Stokes (RANS) flow model. The results showed that this vegetation model offered a significant improvement over rigid vegetation approximations, predicting plant positions and time-averaged flow characteristics. However, the model was very sensitive to the rigidity parameter, which is difficult to parameterise. Furthermore, the model was RANS-based and therefore unable to predict fully time-dependent turbulence characteristics. Recently, Gac (2014) implemented a flexible vegetation model within a large eddy based lattice Boltzmann Model framework, which used a static version of the Euler-Bernoulli beam equation to calculate plant deflection (Kubrak *et al.* 2008). This method reproduced mean velocity profiles well, however the treatment of plant motion did not account for inertial terms, solving only for a steady, static case at each time-step.

It is clear from the above discussion that, as yet, a numerical model does not exist that is capable of predicting the time dependent interaction between flow and plant movement within a high resolution, three dimensional framework. Consequently, none of the above models are suitable for evaluating temporal vortex dynamics within vegetated flows.

The aim of this paper is to develop and evaluate two novel biomechanical vegetation models, implemented within a computational fluid dynamics (CFD) framework, which enable high resolution modelling of flexible vegetation canopies across a range of plant forms. LES is used in order to resolve the large-scale turbulence dynamics. Once the models are described they are then tested against flume data collected with high resolution particle image velocimetry (PIV). The merits of such models in elucidating high resolution flow and plant data are then discussed.

3 Model Development

3.1 Vegetation Conceptualisation

In the approach developed here, vegetation is treated as an immersed boundary, using a dual grid system similar to Ikeda *et al.* (2001) where the vegetation grid and the LES grid interact at each time-step (Fig. 1a). The vegetation is represented as porosity within the LES grid. This builds upon the mass flux scaling algorithm (Lane *et al.* 2002, 2004, Hardy *et al.* 2005) initially developed for modelling flow over complex topographies. This method has been successfully applied across a range of different spatial scales, from millimetre scale sections of gravel beds (Lane *et al.* 2002, Hardy *et al.* 2007) through to kilometre scale large river reaches (Sandbach *et al.* 2012). Here, it is developed further into a dynamic mass flux scaling algorithm, capable of representing plant motion through a time-varying porosity term. Under this scheme, at each time-step, every cell in the numerical domain is assigned a porosity value between 0 and 1 (where 0 is fully blocked and 1 is no blockage) that controls the mass flux though the cell. This approach is similar to the cut-cell method used by Kim and Stoesser (2011) in modelling rigid vegetation canopies. It is also similar to the method employed by Ikeda *et al.* (2001) to model flexible vegetation within a two-dimensional model. The key difference between the model developed below and that of Ikeda *et al.* (2001) is that here the grid resolution is smaller than the vegetation stalk diameter, and therefore the porosity is not used to represent stem density (as in Fig. 1a) but rather to represent volume blockage due to a single stem (Fig. 1b). The vegetation grid and the LES grid interact at each time-step in a sequentially staggered manner (Felippa *et al.* 2001). Velocity and pressure data pass to the plant grid and are used to calculate plant motion before the new plant mass data pass back to the LES grid for the next flow solution. Plant motion is calculated based upon balancing the external forces exerted by the fluid on the vegetation, namely buoyancy and drag, against the internal vegetation rigidity force.

The plant is assumed to comprise discrete components (Fig. 1), where the stem is conceptualised as a set of discrete connected masses. Consequently, at a very fine scale, the vegetation does not retain its shape, although plant mass is preserved (Ikeda *et al.*, 2001). Each discrete component of the stem is treated as a fixed shape; cylinders for the semi-rigid model and cuboids for the highly-flexible model. The centre of mass of the shape is treated as the stem centre, which then moves according to force balance. As the centre of mass moves at each time-step, so the original shape of each plant section is translated and remapped separately. In this initial application we only consider single-stemmed plants without foliage or more complex plant form. However, the approach enables a multitude of individual stems to be modelled simultaneously, allowing the representation of realistic vegetation patches.

3.2 Characterisation of plant form

Aquatic vegetation covers a wide variety of plant species each exhibiting different plant morphologies and biomechanical characteristics. It is not feasible to develop an individual model for each vegetation species but it is necessary to classify and to distinguish between broad vegetation types. In this model development we apply the parameters used by Nikora (2010) and Nepf (2012): (i) the Cauchy number (Eq. 1) which is the ratio of the drag force (Eq. 3) to the plant rigidity force (Eq. 5); and (ii) the buoyancy number (Eq. 2) which represents the ratio between the buoyancy (Eq. 4) and rigidity force:

$$Ca = \frac{F_D}{F_R} \tag{1}$$

$$B = \frac{F_B}{F_R} \tag{2}$$

$$F_D = \frac{1}{2}\rho C_D w_s u^2 l_s \tag{3}$$

$$F_B = (\rho - \rho_s) g w_s t_s l_s \tag{4}$$

$$F_R = EI/l_s^2 \tag{5}$$

These two numbers are a function of both flow characteristics such as fluid density (ρ) and velocity (u) as well as vegetation characteristics such as stalk width (w_s), length (l_s) and thickness (t_s), material density (ρ_s) and flexural rigidity (EI). Nikora (2010) developed a two option classification for aquatic vegetation where vegetation was classified as either tensile or bending dependent upon the Cauchy number, following previous work to parameterise drag and reconfiguration of flexible bodies in fluid flows (e.g. Gosselin *et al.* 2010, Gosselin and de Langre 2011). Luhar and Nepf (2011) extended this single parameter approach by characterising the vegetation behaviour using both the Cauchy and the buoyancy number. Inclusion of the buoyancy number allows the categorisation of the dominant plant response force. They used these two parameters and their ratio ($B^{-1}Ca$), which between them represent the balances between the three key forces (drag, rigidity and buoyancy), to predict plant reconfiguration. This categorisation approach has been shown to be a useful framework within which to characterise the interactions between plants and flow and, in this study, vegetation is classed as either bending ($C \approx 1, B \ll 1$) or tensile ($C \gg 1, B \gg 1$). In reality, the Cauchy and buoyancy numbers represent a spectrum of different force balances beyond these two simple categories; however, this characterisation provides a useful initial framework.

Following Nikora (2010), it is apparent that there is a fundamental biomechanical difference between tensile and bending vegetation and as such we require two different sets of governing equations to predict plant motion. Accordingly, two biomechanical models are developed: one structured on the Euler-Bernoulli beam equation to simulate bending

vegetation; and the other structured on an N-pendula model to simulate tensile vegetation. The approach used for both models is outlined below.

3.3 Euler-Bernoulli beam equation model

The Euler-Bernoulli beam equation solves the deflection of a thin beam under external loading. It represents a simplification of linear elasticity theory and balances the external force against the rigidity force of the beam. It is appropriate for modelling vegetation with high rigidity that is controlled mainly by bending forces (Li and Xie 2011). The Euler-Bernoulli beam equation has been used in previous studies both to model explicit vegetation elements (Ikeda *et al.* 2001) as well as to drive canopy-scale motion models (Erduran and Kutija 2003).

The dynamic version of the Euler-Bernoulli beam equation is shown in Eq. (6). It can be split into 3 terms: a bending stiffness term, an inertial term and an external force term. It is these three forces which must be balanced to ascertain the plant movement and position.

$$\underbrace{\frac{\partial^2}{\partial s^2}\left(EI\frac{\partial^2 \xi(s,t)}{\partial s^2}\right)}_{\text{Bending stiffness}} = \underbrace{-\mu_M \frac{\partial^2 \xi(s,t)}{\partial t^2}}_{\text{Inertial}} + \underbrace{q_x(s,t)}_{\text{External}} \tag{6}$$

The equation assumes that the beam is initially straight and under no external load. Given a load, $q_x(s)$, along the beam, the perpendicular displacement, $\xi(s)$, from this initial straight position at a point s along the beam can then be solved. The flexural rigidity (EI) and mass per unit length (μ_M) are key internal plant properties within the equation. For simplicity and initial development and testing, these have been assumed constant although this is not necessarily the case. Many plants will exhibit variations in flexural rigidity along the stem and it is likely that most vegetation stalks will also differ in diameter along the stalk (Miler *et al.* 2012). This would lead to an s-dependence in both flexural rigidity and mass per unit length. For the mass term this is straightforward and could be implemented at a later stage. However, the flexural rigidity term lies within a differential operator, and therefore adding an s-dependence would alter the numerical scheme considerably. Therefore, the model described below is only valid for stems of constant rigidity. The external load, $q_x(s)$, is calculated from the drag and buoyancy forces acting on the stem (Eqs. 3 and 4).

The equation is solved using an implicit differencing scheme, which guarantees universal stability regardless of spatial and temporal discretisation, and the boundary conditions for a cantilevered beam ($\xi(0,t) = \xi'(0,t) = \xi''(l_s,t) = \xi'''(l_s,t) = 0$) were applied at the fixed and free ends.

A key part in verifying the numerical model is demonstrating that the solution obtained from applying the model is independent of grid discretisation (i.e. grid resolution) (Hardy *et al.* 2005). In order to assess grid independence, steady-state solutions obtained

using different grid resolutions along the stalk were compared (Fig. 2). The results show that at low resolutions, with fewer nodes, there is clear grid dependence. However, as the resolution increases, the grid becomes more independent. For the cases with n>34, the error is less than 2%. Therefore, n was set at 50, so that the vegetation grid discretisation matched the LES grid discretisation, whilst ensuring minimal discretisation error.

3.4 N-pendula model

The N-pendula model is conceptually different to the Euler-Bernoulli beam equation, being a local force balance model rather than a global differential equation based model. The main implication of this is that flexural rigidity and plant position can be considered within a more local context. This leads to a much more flexible model which is ideal for modelling highly flexible vegetation such as aquatic macrophytes (e.g. *Ranunculus penicillatus*).

The model is conceptualised as a series of connected pendula of length l_s (Fig. 3). Each pendulum is subject to a moment about its pivot, which is a combination of the external fluid forces and the internal resistive force in the manner previously used (Abdelrhman 2007, Dijkstra and Uittenbogaard 2010). The torque (F_i^{TOR}) and tension (F_i^{TEN}) forces at each hinge are linked such that:

$$F_i^{TOR} = q_z \cos\theta_i - q_x \sin\theta_i + F_{i+1}^{TEN} \sin(\theta_i - \theta_{i+1}) - EI\partial^2\theta_i/\partial s^2 \quad (7)$$

$$F_i^{TEN} = q_x \cos\theta_i + q_z \sin\theta_i + F_{i+1}^{TEN} \cos(\theta_i - \theta_{i+1}) \quad (8)$$

In these equations, q_x and q_z are the combined external fluid forces due to drag (Eq. 3) and buoyancy (Eq. 4), resolved in the horizontal and vertical directions respectively and θ_i is the angle between the horizontal and the pendulum as marked on Fig. 3. The model calculates the change in angle at each joint up the stem in turn, by resolving the forces at each joint further up the stalk into radial and transversal forces. After each angle change has been calculated, the resulting movement of the sections higher up the stem caused by the angle change lower down is taken into account by an additional drag force ΔF_Dthat is added to the force calculations for subsequent nodes.

The final term in Eq. (7) corresponds to a rigidity term. Initially the model was run with zero rigidity for two reasons. First, the model is designed to replicate vegetation with very low rigidity, and therefore rigidity should not play a major role in determining plant shape. Second, moving to a hinge model such as the N-pendula model creates difficulties in determining accurate rigidity parameters. Rigidity is not automatically related to the second derivative of the curvature as is the case in the Euler-Bernoulli beam model. Instead, a local treatment must be devised and this is less intuitive to relate to the physical characteristics of the vegetation.

However, experiments with zero rigidity highlighted problems with the stability of the model in this setup. With no rigidity or smoothing of forces over nearby joints, individual joints throughout the plant experienced large instantaneous forces. This then initiated a chaotic N-pendula regime whereby joints freely rotated through more than 360 degrees. This is physically unrealistic and so to maintain model stability, a rigidity term was introduced.

Introducing rigidity necessitates a term which is calculated based on the neighbouring hinges. Dijkstra and Uittenbogaard (2010) use such a term in their model, including an internal moment dependent on $\partial\theta/\partial s$ where s is the distance up-stalk. A similar term was implemented into the model presented here, based on a second order central difference scheme about each node. However, as the flexural rigidity of the stem was very low, this force term had little effect on the instability. Instead, instability within the model was linked to high angular velocities within the initial plant reconfiguration. Therefore a damping force was introduced.

The introduction of resistance or damping can be achieved by two different means. It can either be set as a maximum change in angle per time-step, or as a resistive force that is proportional to the velocity. In order to minimise the restriction on the model, and limit parameterisation strictly to the cases where it was required for stability, this damping term was set as a maximum change in angle per time step. In practical terms, this represents a limit on the angular velocity ($\partial\theta_i/\partial t$). The limit was set to the angular velocity at which, assuming constant angular velocity along the stalk, the tip of the stalk would be moving at twice the fluid inlet velocity. Therefore, the restriction should only apply to extreme cases, such as when the plant is initially configuring into a stable position. Applying this velocity limit to the model removed the unrealistic plant motion and provided stable solutions.

Therefore, in the model application, both the rigidity term and the damping restriction were implemented, one as a physical rigidity which in practice had little impact on the mechanics, and one as a stability parameter which was only activated in the initial stages of the model. This modified model offered a more stable solution and a more realistic representation of plant motion without being constrained by global plant curvature.

3.5 Numerical model parameters

Both vegetation models described above were implemented within a finite volume CFD model. A hybrid-upwind differencing scheme was utilised as in Hardy *et al.* (2007) to maximise both order and stability of the solution. The Navier-Stokes Equations were coupled and solved using the SIMPLEST algorithm (Patankar and Spalding 1972). At each time-step, the flow was solved iteratively, until convergence was obtained. The convergence criterion was set such that mass and momentum flux residuals were reduced to 0.1% of the inlet flux.

Flow was simulated using LES with a standard Smagorinsky sub-grid model with $C_S = 0.17$ (Lilly 1967, Schumann 1991). It has been documented that values of C_S may vary between 0.07-0.24 and will be dependent upon local conditions (Rogallo and Moin 1984). However, without *a priori* information regarding the local values of C_S, a single, average term was employed. This follows the work of Gac (2014) who used an averaged constant when applying a similar vegetation model, and showed there was very weak sensitivity to C_S. In order to aid convergence, the simulations were started from a converged steady RANS solution using an RNG κ-ε turbulence model.

4 Model assessment

In order to assess the performance of the two biomechanical models, the data obtained from the models were compared against flume data, obtained from high-resolution flume experiments with both real and artificial vegetation. The Euler-Bernoulli beam equation was validated using artificial stems, whereas the N-pendula model was validated using natural vegetation (*Ranunculus penicillatus*).

4.1 Flume setup

The flume experiments were conducted in a flume 10 m long (l) and 1 m wide (w). The slope was set at a constant value of 0.01 and the depth was set at 0.4 m throughout the measurement section. Velocity data were collected for a 0.3 m long section of the domain using a DANTEC two-dimensional PIV system which is a nonintrusive, whole flow field technique for velocity measurement (Hardy *et al.* 2005). As the focus of this paper is within-canopy flows, any kind of flow measurement is a challenge and requires some sacrifice in the quality of data to be obtained. In particular, whilst intrusive flow measurement devices might be used, they have the disadvantage of perturbing not only the flow, but also the canopy behaviour which is a critical concern of the modelling. Use of PIV has the advantage that, whilst it may lose some representation within the canopy, it does allow quantitative flow visualisation of the entire flow field through time without any flow or canopy intrusion (Hardy *et al.* 2009, 2010) and for this reason it has been proven as a useful method for assessing CFD predictions (Hardy *et al.* 2005). This represents an increase in complexity from most canopy studies which have relied heavily upon point measurements of velocity (e.g. Nepf and Vivoni 2000, Ghisalberti and Nepf 2004), which are not able to provide detailed information regarding flow-vegetation interactions (Okamoto and Nezu 2009).

Measurement is based upon seeding of the flow with neutrally buoyant tracer particles (hollow reflective glass spheres with a mean diameter of 10μm) and illuminating the flow field with a single pulsed Litron Nano laser light sheet. A charge-coupled device (CCD)

camera was positioned perpendicular to the light sheet to capture the illuminated flow field at a temporal resolution of 50 Hz. The downstream and vertical velocity maps were derived by draping a digital mesh of 8 x 8 pixel interrogation regions over the image, where the dimension of each pixel was approximately 0.6 mm. In each interrogation region, a fast Fourier transform (FFT)-based spatial cross-correlation technique was applied to consecutive images to determine both velocity components (Westerweel 1997). In order to maximise the signal-to-noise ratio of the particle cross-correlations in the PIV analysis, six quality checks were applied to the data (Hardy *et al.* 2005) including a 25% overlap between interrogation regions. In addition, an adaptive correlation method was used whereby initially, interrogation regions of size 32 x 32 pixels and subsequently 16 x 16 pixels were used to increase the accuracy of the eventual 8 x 8 pixel cross-correlation. With this methodology, the mean bias error (accuracy) and RMS error (precision) of the derived velocities is in the order of 0.1 pixels (Huang *et al.* 1997) and the uncertainty in the velocity measurements was therefore in the order of 0.003 ms^{-1}. The resulting velocity map had a field of view of 0.52 m by 0.33 m at a spatial resolution of 0.0038 m collected at 50 Hz over a time length of 1 minute to provide a stationary time series. From this data, a suitable 30 s time series was selected for comparison with the model data.

The artificial vegetation used to validate the beam model consisted of Versilic® Peroxide-cured silicone tubing (Fig. 4). The stems were 0.1 m in length with a diameter of 0.005 m. The stems were set out in a staggered layout in line with previous studies (e.g. Dunn *et al.* 1996, Nepf 1999), with 0.05 m separation between stems in the lateral direction and 0.1 m between stems in the downstream direction. This provided a solid volume fraction of $\phi = 0.004$ which is of the same order of magnitude as the sparser canopies used in previous studies, (e.g. Tanino and Nepf 2008), whilst maximising illumination within the canopy and limiting blockage of the flow field. The flexural rigidity of the stems was measured using bending tests as 0.0003 Nm^2.

In order to validate the N-pendula model, flume experiments were undertaken with natural vegetation. Samples of *Ranunculus penicillatus* plants were collected from a local field site on the River Browney, Durham, UK in early September 2011. The vegetation was transported in wet sacks to the laboratory and used in the flume on the same day to limit the effect of changes in plant biomechanics due to the vegetation having been removed from its natural environment and the consequent lack of light and nutrients. The vegetation was fixed to the bed of the flume using cable ties to replicate the natural patch configuration (Fig. 5). It was not possible to measure the flexural rigidity of the natural vegetation, as the force required to bend the vegetation was smaller than the resolution of the force-meter. This indicated the minor role in which flexural rigidity plays in determining plant position for highly flexible plants.

4.2 Numerical setup: Euler-Bernoulli beam model

The Euler-Bernoulli beam model was implemented within a CFD model where the numerical domain was set up to represent a section of the flume experiments described above. Due to the vegetation size, and subsequent limits on grid resolution, it was not possible to represent the full width and length of the domain numerically. Instead, a section 0.5 m long, 0.2 m wide and 0.4 m deep was used. The grid resolution was set as 0.002 m in the downstream and vertical direction and 0.001 m in the lateral direction (nx=250, ny=200, nz=200). The grid was twice as fine in the lateral direction in order to adequately capture the stem-scale wake separation at the lowest possible computational cost. Applying the same vegetation configuration as in the flume experiments, the numerical domain contained 35 individual stems, each with the same properties as those used in the flume experiments. The Euler-Bernoulli beam model was only applied in the *x*-*z* plane. The model could be extended to include motion in the *x*-*y* plane too, but only one dimension was considered for this initial case.

The inlet conditions for the numerical domain were set to match the inlet velocity profile measured in the flume experiment. The Reynolds number of the flow was approximately 14,500 and the Froude number was approximately 0.1. The flow was therefore both fully turbulent and sub-critical throughout the domain. The bed was treated as a no-slip boundary approximated using the log law of the wall while the side walls of the domain were considered frictionless boundaries. The free surface was approximated using a rigid-lid approach, but corrected to achieve the mass conservation following the approach of Bradbrook *et al.* (1998). The flow was simulated at 10 Hz temporal resolution. The temporal resolution was chosen such that it enabled time-efficient simulations that were suitable for validating the flow field within a realistic CPU time frame.

4.3 Numerical setup: N-pendula model

The N-pendula was designed to replicate highly-flexible macrophytes, rather than semi-rigid stalks similar to those used in the artificial vegetation experiments. Therefore, real vegetation was used to validate the N-pendula model. However, the plants used (*Ranunculus penicillatus*) were complex and varied in form, with multiple plants used, each with multiple stems. The N-pendula model is not currently capable of representing such complexities; nevertheless the validation framework used here seeks to assess the model's usefulness at predicting the general characteristics of the canopy flow.

The N-pendula model was implemented within a CFD model with similar boundary conditions and solution method to that used for the Euler-Bernoulli beam model except that a recirculating boundary condition was used in the downstream direction. In this case, the

domain was 0.8 m long, 0.1 m wide and 0.3 m high. The domain length was increased compared to the Euler-Bernoulli beam case due to the longer stem length within the patch. The grid resolution was 0.002 m in each dimension (*nx*=400, *ny*=50, *nz*=150). Due to memory constraints imposed by the use of a longer domain, the domain height had to be limited to 0.3 m, which was 0.1 m shallower than the flume. However, as the vegetation did not enter this portion of the domain within the experiments, this should only have a minor effect on the results. The Reynolds number was 12,000 and the Froude number was approximately 0.16 and therefore the flow was both fully turbulent and sub-critical. This simulation was applied to investigate plant interaction processes as well as for validation and so was run for 30 s at a temporal resolution of 50 Hz. However, for validation purposes, the data were analysed at 10 Hz, consistent with the Euler-Bernoulli beam model results.

The length of the stalks was set equal to 0.15 m which was an estimate of the mean individual stem length of the canopy, with a stem diameter of 6 mm reflecting the mean diameter of stem and associated streamlined foliage within the real vegetation. In this application, pendulum length was set such that each element had equal length, width and height. This was necessary to minimise plant shape distortion as the plant was translated throughout the domain. As a result, the pendulum length was set at 0.006 m, with n=25. The domain contained 300 stalks, tightly packed ($\phi \approx 0.2$) to resemble a natural vegetation patch. As with the Euler-Bernoulli beam model, the stems were restricted to movement only in the *x*-*z* plane.

4.4 Model validation criteria

In order to validate the numerical models, specific validation criteria were developed that considered both the mean and turbulent aspects of the flow. First, individual point measurements with the same geo-location were compared from numerical and experimental data. This is the most straightforward method of model validation, and is particularly useful for identifying spatial regions of the flow where prediction is particularly good or poor or there is any bias in the data from incorrectly prescribed boundary conditions (Ferguson *et al.* 2003, Lane *et al.* 2004).

Second, normalised velocity profiles were used to compare the performance of the models in predicting the mean canopy flow structure. This is a key element of canopy flows as it is the mean structure which dictates the generation and evolution of coherent turbulent structures at the top of the canopy (Nepf and Ghisalberti 2008). The time-averaged downstream velocity (U) and height (z) variables are normalised (Eqs. 9 and 10) using three characteristic mixing layer variables: the depth-averaged mean downstream velocity ($\overline{U}$) , the velocity difference (ΔU), defined as the difference between the mean velocities of the two

regions forming the mixing layer, and the momentum thickness (θ_M) following previous experimental work (Rogers and Moser 1994, Ghisalberti and Nepf 2002, 2006). Here, $\bar{z}$ is the height at which $U(z) = \overline{U}$

$$U^* = \frac{U-\overline{U}}{\Delta U} \quad (9)$$

$$z^* = \frac{z-\bar{z}}{\theta_M} \quad (10)$$

A full description of the normalisation process can be found in Ghisalberti and Nepf (2002). For this analysis, spatially averaged flow profiles were used in order to remove any velocity signal relating to individual canopy elements. The flume profiles were averaged in time, and in the downstream direction. For the numerical profiles, a two-dimensional downstream-vertical (*x*-*z*) measurement plane, similar to that collected using the PIV, was extracted from the midline (*y*/*w*=0.5). This data was then averaged in a similar manner to the flume data. Using the variables θ_M and $\overline{U}$, calculated during the normalisation process, it is possible to estimate the frequency of the Kelvin-Helmholtz instability and therefore the frequency of shear layer vortices, using Eq. (11) (Ho and Huerre 1984, Ghisalberti and Nepf 2002).

$$f_{KH} = 0.032\frac{\overline{U}}{\theta_M} \quad (11)$$

Third, wavelet analysis was used to assess the temporal characteristics (periodicities) of the turbulent structures above the canopy. Wavelet analysis involves the decomposition of a time series into a set of scaled and translated versions of a wavelet function (Hardy *et al.* 2009). The advantage of this technique over other frequency tools such as spectral analysis is that it is applied locally rather than globally and therefore the calculated spectrum retains a temporal dimension as well as a frequency dimension (Farge 1992). It is therefore particularly suitable for analysing time series' which contain intermittency or non-stationary periodicities (Daubechies 1990, Farge 1992). Wavelets have successfully been used previously within turbulent flows in order to detect the presence of large-scale coherent turbulent structures (Farge 1992, Hardy *et al.* 2009, 2010). A full review of wavelet analysis is provided by Torrence and Compo (1998) and only methodological details are included here. In this study, a Morlet wavelet was fitted to data obtained from the canopy top in order to estimate the power present within the data over a range of different scales, at different points throughout the time series. The Morlet wavelet was chosen because of its similarity with the decomposition of turbulent energy from a characteristic eddy (Hardy *et al.* 2009). The resulting wavelet power spectrum highlights regions of periodicity within the data which correspond to turbulent flow structures.

Following Hardy *et al*. (2009) four specific methodological issues arise: (1) reliability issues at the edge of the dataset due to aperiodicity in the data; (2) choice of scales for

analysis; (3) conversion from wavelet scale to Fourier period; and (4) statistical significance testing of wavelet power. First, the wavelet transform is calculated using an inverse Fourier transform, which assumes that the given dataset is periodic on the domain $(-\infty, \infty)$. Therefore, the wavelet transform will contain spurious values at the edges of the interval [0, *t*] where values outside of the measured interval are used to calculate the wavelet power spectrum within the measured interval. This region of error is dependent upon both wavelet scale (a) and the e-folding time which is a measure of scale-dependent wavelet half-width. The Morlet wavelet has an e-folding time of $\sqrt{2}a$ that was used to define data reliability at the edges as a cone of influence, such that any wavelet power that depended upon a value beyond the bounds of the interval [0, *t*] was rejected. Second, it was necessary to specify a discrete set of time scales over which to measure wavelet power. The resolution of the numerical data (10 Hz) and its associated Nyquist frequency (5 Hz) as well as the length of the time series (30 s) dictate that the scales examined should range between 0.2 s and 30 s. Scale resolution is also subject to computational constraint. Accordingly, scales were analysed for 0.1×2^m for values of *m* between 1 and 8, with increments of 0.1, giving a range of scales from 0.2 s to 25.6 s, subject to the cone of influence. This provided high-resolution scale information across the range of interest, excluding only very low frequency periodicities. Thirdly, the wavelet scale is not necessarily equivalent to the Fourier period, which is the equivalent scale measure of interest. Therefore, the wavelet scale was transformed into the equivalent Fourier period prior to visualisation of results (Torrence and Compo 1998). Finally, we determined whether the wavelet power magnitude was statistically significant compared to a background power spectrum (Torrence and Compo, 1998) associated with white noise, which we assumed to be present within the data (Biron *et al.* 1998). Values that were not statistically significant were discarded prior to visualisation.

These three different aspects of model validation were designed to ensure that the model effectively reproduces the mean and turbulent flow dynamics for both spatial and temporal dimensions. In particular, the criteria were designed to assess the models' performance in reproducing the turbulent energy extraction associated with canopy flows.

4.5 Validation Results: Euler-Bernoulli beam model

Initially, the time-averaged downstream (*U*) and vertical (*W*) velocity components are compared. The spot value comparisons (Fig. 6), taken at a random sample of 50 points across the domain, show variation in model performance throughout the domain. The time-averaged downstream velocity comparison shows that overall there is good agreement between the experimental and numerical data, with an *r* value of 0.953. Applying Ordinary Least Squares (OLS) regression to the data (Table 1) gives a line of best fit with gradient 0.93, highlighting

that over the range of velocity values there is a near 1:1 relationship between the CFD and PIV data. In general, the model appears to under-predict the time-averaged velocity compared to the experimental data, which is shown by a clustering of points, following a similar gradient to the line of perfect agreement (1:1), and suggests that there may be some systematic error present within the data. There are a number of clear disparities within the data where the model significantly under-predicts the measured experimental velocity. These points occur predominantly in regions where the velocity is low (< 0.1 ms^{-1}).

In order to distinguish between model performance within different regions of flow, the spot data are categorised according to their height within the domain. This three-fold categorisation splits the domain into a canopy region ($z < h$), a shear layer region ($h < z < 2h$) and a boundary layer region ($z > 2h$) corresponding to the three general flow regimes present in canopy flows (Nezu and Sanjou 2008). This categorisation does not correspond exactly with the physical process regions within the flow, but instead provides a simple way of distinguishing model performance within broadly different flow regions. When a similar regression is performed within each region (Table 2), the boundary layer region data (red triangles) show the best agreement with a 1:1 relationship between the model and flume results, with a regression line gradient of 1.04. The associated r value of 0.809 suggests that the model fits the majority of the data well. As with the entire dataset, there is a clear systematic under-prediction of velocity by the model, as demonstrated by the regression line intercept of 0.011 ms^{-1}.

Within the shear layer region (green) there is poor agreement between the regression gradient (0.386) and the line of perfect fit. However this is skewed by three particular points, with the lowest velocities, which appear erroneously inaccurate compared to the other shear layer values. It is thus suggested that the shear layer data display two distinct trends. For the data towards the upper end of the shear layer, model performance is similar to that for the boundary layer, as demonstrated by the cluster of points which appear to follow a similar trend. However, closer to the canopy top, where the velocity is lower, the interference of individual stems leads to poorer model prediction, as shown by three particular points with high disparity in velocity (0.03-0.05 ms^{-1}). The transition from good to poor prediction occurs over a very short and well defined interval. Obtaining good agreement within this region will be particularly difficult: the shear is very high and so extremely small differences in the position of the canopy between modelled and measured values will lead to extremely large modelled errors.

For the within-canopy values, there is very poor agreement between the model and flume values, with a regression gradient of -0.117 and r value of -0.063. Here, there is less evidence of consistent under-prediction by the model, with a wide spread of data on either side of the 1:1 line. We suggest that most of this disparity is due to error within the PIV data.

Although PIV represents an increase in flow measurement capability compared with single point methods, there are still significant errors particularly with regard to taking measurements within the canopy. The reason for this is two-fold. Firstly, although the stem material was chosen to minimise light refraction through the stems, it is clear from the PIV images that there was significant blockage of light, caused by refraction, thus making the canopy regions of the PIV image darker and reducing the accuracy of the PIV. Secondly, due to refraction of light by the stems and filter width of the laser, the rest of the canopy outside of the measurement plane was partially illuminated. This resulted in additional stems, not within the measurement plane, appearing in the PIV image, providing a static background image within the canopy region and introducing error into the PIV measurements in those regions.

The time-averaged vertical velocity spot data show a consistent under-prediction of vertical velocity within the numerical model throughout the domain with only a few exceptions. Agreement between the numerical and experimental data is poor (Table 1) with a regression gradient of -0.382 and corresponding *r* value of -0.519. For this case, there is no significant improvement in predictive capability when particular areas of the domain are considered individually. This poor level of prediction may be due to limitations of the isotropic turbulence model, as well as specification of the inlet boundary condition, which did not contain vertical turbulent velocity fluctuations. The boundary layer data show a reasonable correlation (r = -0.78) about a regression line with a gradient of -2.55. We suggest that this may be due to a streamwise gradient in vertical velocity throughout the flume domain, which was not present within the CFD data. This may be due to the simplified rigid-lid approach used to model the free surface.

The above discussion emphasises that there are a number of uncertainties in the data used to validate the model as well as the model itself. This is not surprising given the complexity of vegetation-flow interactions. Yet, the results are comparable with previous applications of CFD to laboratory flume studies but using far simpler configurations (e.g. non-moving boundaries, Reynolds averaged) where boundary conditions, notably domain geometry, are much more readily determined. For instance, Bradbrook *et al.* (1998) obtained an r value of 0.97 for the *U*-component of velocity when modelling a zero degree confluence of smooth rectangular channels. Another example was an application to study micro-scale flow processes over individual gravel particles, where Lane *et al.* (2004) reported an r value of 0.95 for the *U*-component of velocity. These studies used acoustic Doppler velocimeters (ADV's) where the measurement volumes are typically 10-25 times the spatial discretisation and consequently complex shear flows are averaged.

These point-wise statistical comparisons provide the most stringent test of model performance. We can also validate the model qualitatively by visually comparing measured

and modelled normalised velocity profiles (Fig. 7). These show that the model agrees well geometrically with the flume data as well as with the idealised hyperbolic tangent profile (Ho and Huerre 1984, Ghisalberti and Nepf 2006), which characterises vegetated shear layers, and emphasise that at least some of the quantitative error described above will arise from small errors in the calculated position of the zones of strongest shear. Both the flume and model profiles show a slight asymmetry about the centre of shear layer, compared to the idealised profile. This may be due to the fact that the submergence ratio (H/h~4) meant there was greater depth available for shear layer formation above the canopy than within the canopy. The two full velocity profiles (Fig. 8) show this slight difference in shear layer velocity gradient either side of the canopy top (h~0.1). This figure also highlights the consistent under-prediction of velocity by the model, approximately equal to 0.01 ms^{-1}. This may be due to error within the specification of the upstream boundary condition within the model.

The final part of the validation considers the temporal periodicities. The wavelet plots for the flume and model (Fig. 9) both highlight a range or periodicities present within the flow. These have been broadly classed into 3 scales. First, as most evident in the flume spectra, there are some low time-scale (high frequency) periodicities, typically with frequencies greater than 1Hz (labelled C in Fig. 9). Based upon the stem diameter and the average canopy flow velocity of 0.03-0.05 ms^{-1}, the stem vortex shedding frequency (f=0.2U/w_l) is approximately 1-2 Hz and therefore we argue that these periodicities relate to stem-scale wake-shedding processes. Secondly, there are very large-scale (low-frequency) structures (< 0.2 Hz) present within both the flume and model results (labelled A in Fig. 9), which we argue correspond to domain-induced width-scaling secondary circulation (Hardy *et al.* 2009).

Thirdly, there are medium-scale periodicities, with frequencies between 1-5 Hz which correspond to canopy shear layer generated vortices (labelled B in Fig. 9). The frequency of these vortices is dependent on the flow and canopy conditions and therefore this range will vary accordingly. As outlined in Section 4.1, it is possible to estimate the Kelvin-Helmholtz vortex frequency from the normalised velocity profile characteristics (Eq. 11). The estimated frequencies (Table 3) are plotted in black on both the wavelet spectra. The values are similar in magnitude, which highlights the accuracy with which the numerical model is predicting the dominant canopy-scale turbulence length scale.

Both wavelet plots show periodicities with high wavelet power, at and around the frequencies estimated using Eq. (11) (0.419/0.555 Hz). For the numerical model, there is a strong periodicity present, at a relatively constant frequency which agrees very well with the predicted frequency. The wavelet power magnitude does vary through time, suggesting a time-varying strengthening and weakening of the canopy-layer signal, however, it is present throughout the simulation, following an initial configuration period (~6 s).

For the flume case, the wavelet power is less strong than the numerical model case and this is expected given the additional level of turbulent noise present within the flume experiments. However, there is still a strong periodicity, which is more variable in terms of scale throughout the time series, and which occurs at a slightly lower frequency than that estimated from the velocity profile. It is more similar in frequency to that estimated for, and evident within, the model wavelet spectra. This suggests that the normalised velocity profile is a poorer predictor for the flume experiments. This may be due to the influence of erroneous data within the canopy on the velocity profile. Therefore, it can be seen that despite the small difference in predicted shear-layer vortex frequency (Table 3) the numerical model reproduces the shear layer vortices present within the flume data well.

4.6 Validation Results: N-pendula model

Due to the fact that the flume experiments were not directly analogous to the model simulations, spot values are not compared for this case. Thus, this represents a more qualitative validation; however, this is appropriate given the simplicity of the model compared with the complexity associated with the natural plant forms.

The normalised velocity profiles (Fig. 10) show agreement in both geometry and magnitude of the profiles, both exhibiting the classic s-shaped velocity profile which characterises shear layers. There is a noticeable difference in the shape of the shear layer above and below the canopy top in the numerical simulation. This deviation from both the experimental and idealised profiles is due to asymmetry of the shear layer about the canopy top and may be due to the high stem density and relatively small canopy height.

The two wavelet spectra (Fig. 11) show a much more complex pattern of periodicities within the flow than in the Euler-Bernoulli beam model case. Here, within both spectra there is still evidence of three scales of periodicity, at broadly similar ranges to those described above. However, there is also far more evidence of variability in frequency through time as well as interaction and potentially coalescence between the different periodicities.

Compared to the Euler-Bernoulli beam model data there is more power contained within the smaller time-scales relative to the rest of the spectrum, and this particular periodicity appears to cover a wider range of frequencies up to ~2 Hz. In places, within both spectra, this periodicity appears to coincide with a larger scale periodicity (circled in Figure 11), potentially related to the shear-layer. Particularly, within the flume spectra, this larger-scale periodicity occurs at a frequency very similar to that estimated using Eq. (8) (Table 4), though the frequency is variable through time. The model data displays a different scale periodicity, which agrees less well with the estimated frequency (Table 4). In fact, there

appear to be two periodicities that could relate to the shear-scale vortices: one above and one below the estimated periodicity.

Finally, both the model and experimental data show evidence of low frequency periodicities, though as with the other scales, these are less well defined in terms of frequency than the earlier case. From the wavelet analysis, it is clear that the N-pendula performs less well in exactly reproducing the vortex frequencies evident within the experimental data. However, the model does reproduce an increased variability in frequency and interaction between the different scales of periodicity. Thus we argue that, despite the vast difference in complexity between the real vegetation experiments and the N-pendula model simulation, the model does reproduce key characteristics of the flow dynamics.

5 Preliminary results

Following the formal validation experiments, the vegetation model application was expanded to apply a sensitivity analysis to a range of different canopy conditions. This enabled investigation of conditions beyond those possible within the flume. Here we present two additional sets of results that help to qualitatively evaluate the models' ability to reproduce canopy flow conditions.

Firstly, we present results from an Euler-Bernoulli beam canopy simulation (Fig. 12) with a longer domain (1 m) and higher canopy density ($\phi = 0.098$) than that used in the validation experiments. The increased canopy length enabled the development of vortices over a longer timescale without disruption due to recirculation. Furthermore, the increased canopy density strengthens the drag discontinuity at the canopy top leading to a stronger shear layer (Nepf and Ghisalberti 2008). The solution methods and boundary conditions used within this model were the same as the validation experiments outlined above, except that we used recirculating boundaries in the downstream direction.

Using both Eulerian (Q, λ) and Lagrangian (FTLE) vortex detection methods (Hunt *et al.* 1988, Jeong and Hussain 1995, Haller 2000), it is possible to detect the presence of canopy-scale vortices along the canopy top. Both Eulerian methods identify vortices consistent with canopy shear layer roller vortices (Fig. 13). The FTLE results suggest that the structure may relate to hairpin vortices (Green *et al.* 2007), associated with Finnigan *et al.*'s (2009) canopy flow model. However, due to the narrow width of the domain it is not possible with any certainty to deduce whether this is a roller or hairpin vortex. These vortex detection results also enable the calculation of vortex growth rate through time. For a canopy shear layer, this growth rate can be approximated as the growth of the shear layer thickness (δ), which can be calculated based upon velocity profile characteristics, ΔU and $\overline{U}$ (Eq. 12).

$$\frac{d\delta}{dx} = \alpha . \frac{\Delta U}{\overline{U}} \tag{12}$$

The term α is constant with values between 0.06 and 0.12 depending on initial conditions (Pope 2000). Following Sukhodolova and Sukhodolov (2012), a value of 0.09 has been used here. The change in vortex thickness through time, as measured using the Q and λ_2 criterion (Fig. 14), indicates linear vortex growth at a rate that agrees well with the predicted mixing layer growth rate using Eq. (12). Both criteria show a consistent rate of growth, though the Q criterion suggests a consistently larger vortex thickness. This is because in two-dimensional vortex detection, λ_2 is a subset of Q (i.e. Q is a less discriminative vortex detection method). The agreement in growth rate in Fig. 14 implies that the model is capable of reproducing a vegetated shear layer, consistent with existing theory and observations within the literature.

Secondly, we present an additional analysis of the wavelet spectra presented in Section 4.6. For the purposes of validation, the simulation data was analysed at a frequency of 10 Hz in order to maintain consistency with the Euler-Bernoulli beam equation case. However, both the flume and numerical data were collected at 50 Hz and therefore here we analyse the wavelet spectra obtained from the higher resolution time series (Fig. 15).

Increasing the temporal resolution reveals a more detailed picture of the periodicities within the flow. The flume spectra further shows the existence of a number of different scales of periodicity, from stem-scale high frequency, through to very low frequency patterns. What is clearer in this higher resolution image is the linkages between these scales of periodicity. In contrast to the Euler-Bernoulli beam canopy simulation, the scales are not distinct and there is a large amount of interaction between periodicities across the entire scale-range. This pattern is amplified within the N-pendula simulation, where scale linkages contain more wavelet power, and periodicities appear to coalesce and split through time (dotted lines on Figure 15).

6 Discussion

Model validation shows that, overall, both models predict both the spatial and the temporal characteristics of the mean flow and turbulent dynamics of the canopy system as previously described in experimental results (e.g. Ikeda and Kanazawa 1996, Ghisalberti and Nepf 2002, 2006, Nezu and Sanjou 2008). For example, it has been shown that for a given stem density, both models are able to simulate the extraction of energy from the mean flow at the stem-scale (Zong and Nepf 2010), which leads to the drag discontinuity and associated inflected velocity profile (Ikeda and Kanazawa 1996, Nepf 2012). The shape of the inflected velocity profile agrees well with that associated with a mixing layer (Ho and Huerre 1984) as previously observed in vegetation canopies (Ghisalberti and Nepf, 2002; 2006). Similar to previous studies (Ghisalberti and Nepf, 2002, Ho and Huerre, 1984), the normalised velocity profiles were used to predict the frequency of Kelvin-Helmholtz shedding. The similarity in magnitude between the predicted vortex frequencies from the flume and numerical results

indicates that at a canopy-scale, this energy extraction method is being modelled appropriately.

Within this study, wavelet analysis was used to identify the scale of vortices within the flow. To our knowledge, this is the first time wavelet analysis has been employed within vegetated flows. Previous studies that have used spectral analysis to identify dominant frequencies within the flow (e.g. Ghisalberti and Nepf, 2002; Okamoto and Nezu, 2009). Ghisalberti and Nepf (2002) found good agreement between the observed spectral peak and the predicted Kelvin-Helmholtz frequency. Similar agreement is evident in this application and has been shown within the wavelet spectra and predicted Kelvin-Helmholtz frequencies. This has been particularly well demonstrated for the Euler-Bernoulli beam model simulation, which was most analogous to previous experimental setups (Ghisalberti and Nepf, 2002). The advantage of wavelet analysis demonstrated here is that it illustrates the variability in vortex frequency throughout the duration of the simulation. This is particularly evident in the N-pendula model, but is also present within the artificial vegetation experiments.

One problem that has been highlighted in this study is the difficulty of obtaining high-resolution, temporally continuous, whole flow field measurements of flow over both artificial and natural canopies. Previous work on studying fluvial flows in flumes has shown PIV to be a reliable methodology (Hardy *et al.* 2009, Cooper and Tait 2010a, 2010b, Hardy *et al.* 2010, Hardy *et al.* 2011). The application of PIV in this study, however, has not allowed the full interrogation of the canopy due to issues with illumination. Furthermore, using this experimental setup, it was not possible to measure plant motion, and therefore it is not possible to validate the plant movement component of the biomechanical model. Validation is only achievable through the product of plant movement and its influence on flow. Such aspects of the model performance require further testing and validation and we are currently devising new methodologies to improve the validation procedure.

The results show the numerical models are able to capture high resolution flow dynamics in a manner not currently possible experimentally in flume and field environments. Furthermore, the results suggest the novel approach provides a useful tool for investigating flow structure and plant-flow interactions at high spatial and temporal resolution. The results from the N-pendula model highlight the complexity of interactions within real vegetation canopies and suggest coalescence between turbulent scales that is not included within the current canopy model. Furthermore, a wider range of turbulence scales has been identified within the canopy which supports the conceptual model of Nikora (2010).

Although, the initial application of the model has been on relatively simple canopies, the new methodology presented here enables investigation of flow through complex canopies across a wide range of plant forms. This is essential as natural macrophyte canopies do not conform to the idealised canopy configurations traditionally studied (Dunn *et al.* 1996,

Stoesser *et al.* 2010) and it is possible that different turbulent processes dominate in the non-idealised case. The application of the N-pendula model permits the investigation of turbulent energy extraction, and thus the effect on the mean flow conditions through realistic canopies. The development of these two biomechanical models within a CFD framework provides a promising methodology for investigating key topics within canopy flows such as the nature of vegetative drag and its relationship with flow velocity, the role of feedbacks between flow and vegetation, and the role of plant form and biomechanics in determining canopy flow structure at a scale hitherto not possible.

However, to realise this potential, the models still require further development. Firstly, the models are currently only able to represent single-stem plants of relatively simple morphology. The single-stem limitation can in some instances be countered by the use of multiple plants in close proximity, however, complex plant form and foliage may have a significant impact upon canopy dynamics (Jarvela 2002). Secondly, the models are not able to represent plant-plant collisions, which have been shown to have a significant effect on canopy behaviour (Doare *et al.* 2004). Both improvements are currently being developed.

7 Conclusions

The new biomechanical-CFD models outlined in this paper provide a methodology for understanding flow and turbulence dynamics for vegetation-flow interactions in a fluvial environment. The approach developed here extends a mass flux scaling algorithm originally developed for including complex topography into CFD models (Lane *et al.* 2002, 2004, Hardy *et al.* 2005) and transforms it into a dynamic immersed boundary technique that is coupled in a sequentially staggered manner (Felippa *et al.* 2001). Due to the range of characteristics of different aquatic vegetation, two separate biomechanical models were developed following the classification of Nikora (2010). For bending plants ($C \approx 1, B \ll 1$) a model structured on the Euler-Bernoulli beam equation has been proposed while for tensile plants ($C \gg 1, B \gg 1$) an N-pendula model has been developed. These approaches consider vegetation as a dynamically moving blockage that is coupled to the three-dimensional time dependent flow, and therefore, the model is a step change compared to the existing models of plant-flow interactions.

The spot value comparisons from the model and flume data show that the quantitative detail of the model is reasonable, but is confounded by difficulties in geo-location, specification of boundary conditions and problems obtaining accurate experimental measurements within the canopy. However, qualitative assessment of the models, through analysis of normalised velocity profiles and wavelet spectra, is very promising and suggests that the models replicate the key features of canopy flows. Namely, the models reproduce the

characteristic inflection point in the velocity profile, the subsequent development of a canopy shear layer and the generation of canopy-scale roller vortices. Thus, we suggest this provides a promising methodology for investigating more complex canopy flows for which we do not have a full process understanding.

Acknowledgements

The authors wish to thank Dr Gareth Keevil, the experimental officer at Sorby Environmental Fluid Dynamics Laboratory, University of Leeds for help with the flume experiments. The authors would also like to thank the Associate Editor and 3 anonymous referees whose comments have improved this manuscript. Data presented in this paper can be obtained by contacting the first author.

Funding

First author was funded under NERC PhD studentship and NERC Grant NE/K003194/1. The flume experiments were funded through UK NERC grant NE/ F010060/1.

Notation

a = wavelet scale (s)
B = buoyancy number (-)
Ca = Cauchy number (-)
C_D = drag coefficient (-)
C_S = Smagorinsky constant (-)
EI = flexural rigidity (Nm^2)
f_{KH} = frequency of Kelvin-Helmholtz instability (Hz)
F_i^{TEN} = tensional force at node i (N)
F_i^{TOR} = torque force at node i (N)
g = gravitational acceleration (ms^{-2})
H = water depth (m)
h = canopy height (m)
l = domain length (m)
l_s = stalk length (m)
n = number of nodes (-)
nx = number of grid cells in downstream direction (-)
ny = number of grid cells in lateral direction (-)
nz = number of grid cells in vertical direction (-)

q_x = horizontal component of the external force (N)

q_z = vertical component of the external force (N)

r = correlation coefficient (-)

s = up-stem coordinate (m)

t = time (s)

t_s = stalk thickness (m)

u = instantaneous downstream velocity (ms^{-1})

U = time-averaged downstream velocity (ms^{-1})

$\overline{U}$ = mean mixing layer velocity (ms^{-1})

U^* = normalised velocity (-)

w_s = stalk width (m)

w = domain width (m)

W = time-averaged vertical velocity (ms^{-1})

x = downstream coordinate (m)

y = lateral coordinate (m)

z = vertical coordinate (m)

$\bar{z}$ = height at which $U = \overline{U}$

z^* = normalised height (-)

α = constant (-)

ΔU = mixing layer velocity difference (ms^{-1})

δ = shear layer thickness (m)

θ_M = momentum thickness (m)

θ_i = angle to the horizontal at node I (-)

μ_M = mass per unit length (kgm^{-1})

ξ = plant displacement (m)

ρ = water density (kgm^{-3})

ρ_s = material density (kgm^{-3})

ϕ = solid volume fraction (-)

References

Abdelrhman, M. A. (2007). Modeling coupling between eelgrass Zostera marina and water flow. *Mar. Ecol-Prog. Ser.*, 338, 81-96.

Biron, P. M., Lane, S. N., Roy, A. G., Bradbrook, K. F., Richards, K. S. (1998). Sensitivity of bed shear stress estimated from vertical velocity profiles: the problem of sampling resolution. *Earth Surf. Process. Landforms*, 23(2), 133-139.

Bradbrook, K. F., Biron, P. M., Lane, S. N., Richards, K. S., Roy, A. G. (1998). Investigation of controls on secondary circulation in a simple confluence geometry using a three-dimensional numerical model. *Hydrol. Process.*, 12(8), 1371-1396.

Cooper, J. R., Tait, S. J. (2010a). Examining the physical components of boundary shear stress for water-worked gravel deposits. *Earth Surf. Process. Landforms*, 35(10), 1240-1246.

Cooper, J. R., Tait, S. J. (2010b). Spatially representative velocity measurement over water-worked gravel beds. *Water Resour. Res.*, 46(11), W11559.

Daubechies, I. (1990). The wavelet transform time-frequency localization and signal analysis. *IEEE Trans. inform. Theory*, 36, 961-1004.

Defina, A., Bixio, A. C. (2005). Mean flow and turbulence in vegetated open channel flow. *Water Resour. Res.*, 41(7), 12.

Dijkstra, J. T., Uittenbogaard, R. E. (2010). Modeling the interaction between flow and highly flexible aquatic vegetation. *Water Resour. Res.*, 46(12), W12547.

Doare, O., Moulia, B., Langre, E. d. (2004). Effect of Plant Interaction on Wind-Induced Crop Motion. *J. Biomech. Eng.*, 126(2), 146-151.

Dunn, C., Lopez, F., Garcia, M. H. (1996). Mean flow and turbulence in a laboratory channel with simulated vegetation *Hydrosystems laboratory hydraulic engineering series*. Urbana: University of Illinois.

Erduran, K. S., Kutija, V. (2003). Quasi-three-dimensional numerical model for flow through flexible, rigid, submerged and non-submerged vegetation. *J. Hydroinform.*, 5(3), 189-202.

Farge, M. (1992). Wavelet Transforms and their Applications to Turbulence. *Ann. Rev. Fluid Mech.*, 24(1), 395-458.

Felippa, C. A., Park, K. C., Farhat, C. (2001). Partitioned analysis of coupled mechanical systems. *Comput. Meth. Appl. Mech. Eng.*, 190(24-25), 3247-3270.

Ferguson, R. I., Parsons, D. R., Lane, S. N., Hardy, R. J. (2003). Flow in meander bends with recirculation at the inner bank. *Water Resour. Res.*, 39(11), 1322.

Finnigan, J. (2000). Turbulence in Plant Canopies. *Ann. Rev. Fluid Mech.*, 32(1), 519-571.

Finnigan, J. J., Shaw, R. H., Patton, E. G. (2009). Turbulence structure above a vegetation canopy. *J. Fluid Mech.,* 637, 387-424.

Fischer-Antze, T., Stoesser, T., Bates, P., Olsen, N. R. B. (2001). 3D numerical modelling of open-channel flow with submerged vegetation. *J. Hydraul. Res.,* 39(3), 303-310.

Gac, J. (2014). A large eddy based lattice-Boltzmann simulation of velocity distribution in an open channel flow with rigid and flexible vegetation. *Acta Geophysica,* 62(1), 180-198.

Ghisalberti, M., Nepf, H. M. (2002). Mixing layers and coherent structures in vegetated aquatic flows. *J. Geophys. Res.-Oceans,* 107(C2), 11.

Ghisalberti, M., Nepf, H. M. (2004). The limited growth of vegetated shear layers. *Water Resour. Res.,* 40(7), W07502.

Ghisalberti, M., Nepf, H. M. (2006). The Structure of the Shear Layer in Flows over Rigid and Flexible Canopies. *Environ. Fluid Mech.,* 6(3), 277-301.

Gosselin, F., de Langre, E., Machado-Almeida, B. A. (2010). Drag reduction of flexible plates by reconfiguration. *J. Fluid Mech.,* 650, 319-341.

Gosselin, F. P., de Langre, E. (2011). Drag reduction by reconfiguration of a poroelastic system. *J. Fluids Structures,* 27(7), 1111-1123.

Green, M. A., Rowley, C. W., Haller, G. (2007). Detection of Lagrangian coherent structures in three-dimensional turbulence. *J. Fluid Mech.,* 572, 111-120.

Gurnell, A. (2014). Plants as river system engineers. *Earth Surf. Process. Landforms,* 39(1), 4-25.

Haller, G. (2000). Finding finite-time invariant manifolds in two-dimensional velocity fields. *Chaos: An Interdisciplinary Journal of Nonlinear Science,* 10(1), 99-108.

Hardy, R. J., Best, J. L., Lane, S. N., Carbonneau, P. E. (2009). Coherent flow structures in a depth-limited flow over a gravel surface: The role of near-bed turbulence and influence of Reynolds number. *J. Geophys. Res.-Earth Surf.,* 114, 18.

Hardy, R. J., Best, J. L., Lane, S. N., Carbonneau, P. E. (2010). Coherent flow structures in a depth-limited flow over a gravel surface: The influence of surface roughness. *J. Geophys. Res.-Earth Surf.,* 115.

Hardy, R. J., Best, J. L., Parsons, D. R., Keevil, G. M. (2011). On determining the geometric and kinematic characteristics of coherent flow structures over a gravel bed: a new approach using combined PLIF-PIV. *Earth Surf. Process. Landforms,* 36(2), 279-284.

Hardy, R. J., Lane, S. N., Ferguson, R. I., Parsons, D. R. (2007). Emergence of coherent flow structures over a gravel surface: A numerical experiment. *Water Resour. Res.,* 43(3), 14.

Hardy, R. J., Lane, S. N., Lawless, M. R., Best, J. L., Elliott, L., Ingham, D. B. (2005). Development and testing of a numerical code for treatment of complex river channel topography in three-dimensional CFD models with structured grids. *J. Hydraul. Res.,* 43(5), 468-480.

Haslam, S., Sinker, C., Wolseley, P. (1975). British Water Plants. *Field Studies,* 4, 243-351.

Ho, C. M., Huerre, P. (1984). Perturbed Free Shear Layers. *Ann. Rev. Fluid Mech.,* 16, 365-424.

Huang, H., Dabiri, D., Gharib, M. (1997). On errors of digital particle image velocimetry. *Meas. Sci. Technol.,* 8(12), 1427-1440.

Hunt, J. C. R., Wray, A. A., Moin, P. (1988). Eddies, stream and convergence zones in turbulent flows *Center for Turbulence Research Report* (Vol. CTR-S88, pp. 193-208).

Ikeda, S., Kanazawa, M. (1996). Three-dimensional organized vortices above flexible water plants. *J. Hydraul. Eng.,* 122(11), 634-640.

Ikeda, S., Yamada, T., Toda, Y. (2001). Numerical study on turbulent flow and honami in and above flexible plant canopy. *International Journal of Heat and Fluid Flow,* 22(3), 252-258.

Jarvela, J. (2002). Flow resistance of flexible and stiff vegetation: a flume study with natural plants. *J. Hydrology,* 269(1-2), 44-54.

Jeong, J., Hussain, F. (1995). On the identification of a vortex. *J. Fluid Mech.,* 285, 69-94.

Kadlec, R. (1990). Overland Flow in Wetlands: Vegetation Resistance. *J. Hydraul. Eng.,* 116(5), 691-706.

Kemp, J. L., Harper, D. M., Crosa, G. A. (2000). The habitat-scale ecohydraulics of rivers. *Ecological Engineering,* 16(1), 17-29.

Kim, S. J., Stoesser, T. (2011). Closure modeling and direct simulation of vegetation drag in flow through emergent vegetation. *Water Resour. Res.,* 47(10), W10511.

Kubrak, E., Kubrak, J., Rowiński, P. M. (2008). Vertical velocity distributions through and above submerged, flexible vegetation. *Hydrolog. Sci. J.,* 53(4), 905-920.

Lane, S. N., Bradbrook, K. F., Richards, K. S., Biron, P. A., Roy, A. G. (1999). The application of computational fluid dynamics to natural river channels: three-dimensional versus two-dimensional approaches. *Geomorphology,* 29(1–2), 1-20.

Lane, S. N., Hardy, R. J., Elliott, L., Ingham, D. B. (2002). High-resolution numerical modelling of three-dimensional flows over complex river bed topography. *Hydrol. Process.,* 16(11), 2261-2272.

Lane, S. N., Hardy, R. J., Elliott, L., Ingham, D. B. (2004). Numerical modeling of flow processes over gravelly surfaces using structured grids and a numerical porosity treatment. *Water Resour. Res.,* 40(1), 18.

Li, C. W., Xie, J. F. (2011). Numerical modeling of free surface flow over submerged and highly flexible vegetation. *Adv. Water Resour.,* 34(4), 468-477.

Lilly, D. K. (1967). *The representation of small-scale turbulence in numerical simulation experiments.* IBM Scientific Computing Symp. on Environmental Sciences.

Liu, C., Shen, Y.-m. (2008). Flow structure and sediment transport with impacts of aquatic vegetation. *J. Hydrodyn.*, 20(4), 461-468.

Liu, D., Diplas, P., Fairbanks, J. D., Hodges, C. C. (2008). An experimental study of flow through rigid vegetation. *J. Geophys. Res.*, 113.

López, F., García, M. (1998). open-channel flow through simulated vegetation: Suspended sediment transport modeling. *Water Resour. Res.*, 34(9), 2341-2352.

Lopez, F., Garcia, M. H. (2001). Mean flow and turbulence structure of open-channel flow through non-emergent vegetation. *J. Hydraul. Eng.*, 127(5), 392-402.

Luhar, M., Nepf, H. M. (2011). Flow-induced reconfiguration of buoyant and flexible aquatic vegetation. *Limnol. Oceanogr.*, 56(6), 2003-2017.

Miler, O., Albayrak, I., Nikora, V., O'Hare, M. (2012). Biomechanical properties of aquatic plants and their effects on plant-flow interactions in streams and rivers. *Aquat. Sci.*, 74(1), 31-44.

Naden, P., Rameshwaran, P., Mountford, O., Robertson, C. (2006). The influence of macrophyte growth, typical of eutrophic conditions, on river flow velocities and turbulence production. *Hydrol. Process.*, 20(18), 3915-3938.

Nepf, H., Ghisalberti, M. (2008). Flow and transport in channels with submerged vegetation. *Acta Geophysica*, 56(3), 753-777.

Nepf, H., Ghisalberti, M., White, B., Murphy, E. (2007). Retention time and dispersion associated with submerged aquatic canopies. *Water Resour. Res.*, 43(4), 10.

Nepf, H. M. (1999). Drag, turbulence, and diffusion in flow through emergent vegetation. *Water Resour. Res.*, 35(2), 479-489.

Nepf, H. M. (2012). Hydrodynamics of vegetated channels. *J. Hydraul. Res.*, 50(3), 262-279.

Nepf, H. M., Vivoni, E. R. (2000). Flow structure in depth-limited, vegetated flow. *J. Geophys. Res.-Oceans*, 105(C12), 28547-28557.

Nezu, I., Sanjou, M. (2008). Turburence structure and coherent motion in vegetated canopy open-channel flows. *J. Hydro-env. Res.*, 2(2), 62-90.

Nikora, V. (2010). Hydrodynamics of aquatic ecosystems: An interface between ecology, biomechanics and environmental fluid mechanics. *River Res. Appl.*, 26(4), 367-384.

Okamoto, T.-A., Nezu, I. (2009). Turbulence structure and "Monami" phenomena in flexible vegetated open-channel flows. *J. Hydraul. Res.*, 47, 13.

Patankar, S. V., Spalding, D. B. (1972). A calculation procedure for heat, mass and momentum transfer in three-dimensional parabolic flows. *Int. J. Heat Mass Trans.*, 15(10), 1787-1806.

Pope, S. B. (2000). *Turbulent Flows*. Cambridge University Press, Cambridge.

Raupach, M. R., Finnigan, J. J., Brunet, Y. (1996). Coherent eddies and turbulence in vegetation canopies: The mixing-layer analogy. *Bound.-Layer Meteor.*, 78(3-4), 351-382.

Rogallo, R. S., Moin, P. (1984). Numerical Simulation of Turbulent Flows. *Ann. Rev. Fluid Mech.*, 16(1), 99-137.

Rogers, M. M., Moser, R. D. (1994). Direct simulation of a self-similar turbulent mixing layer. *Phys. Fluids*, 6(2), 903-923.

Sand-Jensen, K. (1998). Influence of submerged macrophytes on sediment composition and near-bed flow in lowland streams. *Freshw. Biol.*, 39(4), 663-679.

Sand-Jensen, K. A. J., Jeppesen, E., Nielsen, K., Van Der Bijl, L., Hjermind, L., Nielsen, L. W., Ivlrsln, T. M. (1989). Growth of macrophytes and ecosystem consequences in a lowland Danish stream. *Freshw. Biol.*, 22(1), 15-32.

Sandbach, S. D., Lane, S. N., Hardy, R. J., Amsler, M. L., Ashworth, P. J., Best, J. L., Nicholas, A. P., Orfeo, O., Parsons, D. R., Reesink, A. J. H., Szupiany, R. N. (2012). Application of a roughness-length representation to parameterize energy loss in 3-D numerical simulations of large rivers. *Water Resour. Res.*, 48(12), W12501.

Schulz, M., Kozerski, H.-P., Pluntke, T., Rinke, K. (2003). The influence of macrophytes on sedimentation and nutrient retention in the lower River Spree (Germany). *Water Res.*, 37(3), 569-578.

Schumann, U. (1991). Direct and large eddy simulation of turbulence: Summary of the state-of-the-art 1991 *Lecture Series 1991-02: Introduction to the modelling of turbulence*. Brussels: Von Karman Institute.

Siniscalchi, F., Nikora, V. I. (2012). Flow-plant interactions in open-channel flows: A comparative analysis of five freshwater plant species. *Water Resour. Res.*, 48(5), W05503.

Stoesser, T., Kim, S. J., Diplas, P. (2010). Turbulent Flow through Idealized Emergent Vegetation. *J. Hydraul. Eng.*, 136(12), 1003-1017.

Stoesser, T., Liang, C., Rodi, W., Jirka, G. (2006). Large eddy simulation of fully-developed turbulent flow through submerged vegetation *River Flow 2006, Two Volume Set*. Taylor & Francis.

Sukhodolov, A. N., Sukhodolova, T. A. (2010). Case Study: Effect of Submerged Aquatic Plants on Turbulence Structure in a Lowland River. *J. Hydraul. Eng.*, 136(7), 434-446.

Sukhodolov, A. N., Sukhodolova, T. A. (2012). Vegetated mixing layer around a finite-size patch of submerged plants: Part 2. Turbulence statistics and structures. *Water Resour. Res.*, 48(12), W12506.

Sukhodolova, T. A., Sukhodolov, A. N. (2012). Vegetated mixing layer around a finite-size patch of submerged plants: 1. Theory and field experiments. *Water Resour. Res.*, 48(10), W10533.

Tanino, Y., Nepf, H. (2008). Laboratory Investigation of Mean Drag in a Random Array of Rigid, Emergent Cylinders. *J. Hydraul. Eng.*, 134(1), 34-41.

Torrence, C., Compo, G. P. (1998). A Practical Guide to Wavelet Analysis. *Bulletin of the American Meteorological Society*, 79(1), 61-78.

Westerweel, J. (1997). Fundamentals of digital particle image velocimetry. *Meas. Sci. Technol.*, 8(12), 1379-1392.

Wilson, C., Stoesser, T., Bates, P. D., Pinzen, A. B. (2003). Open channel flow through different forms of submerged flexible vegetation. *J. Hydraul. Eng.*, 129(11), 847-853.

Yagci, O., Kabdasli, M. S. (2008). The impact of single natural vegetation elements on flow characteristics. *Hydrol. Process.*, 22(21), 4310-4321.

Zong, L., Nepf, H. (2010). Flow and deposition in and around a finite patch of vegetation. *Geomorphology*, 116(3–4), 363-372.

Table 1 Ordinary Least Squares Regression statistics for the whole domain for the Euler-Bernoulli beam experiments

Velocity Component	Intercept (ms^{-1})	Gradient	*r*
Downstream (*U*)	-0.001	0.930	0.953
Vertical (*W*)	-0.001	-0.382	-0.519

Table 2 Ordinary Least Squares Regression statistics for different regions of the domain. The three regions correspond to those in Fig. 6 (i.e. canopy=blue crosses, shear=green circles, boundary=red triangles)

Velocity Component	Intercept (ms^{-1})	Gradient	*r*
U canopy	0.031	-0.117	-0.063
U shear	0.117	0.386	0.834
U boundary	0.011	1.040	0.809
W canopy	0.011	0.273	0.184
W shear	0.005	0.049	0.032
W boundary	0.001	-2.550	-0.780

Table 3 Normalised velocity profile characteristics for the semi-rigid vegetation. $\overline{U}$ is the mean shear layer velocity, θ_M is the shear layer momentum thickness and f_{KH} is the predicted Kelvin-Helmholtz frequency using Eq. (8)

	$\overline{U}$ (ms^{-1})	θ_M (m)	f_{KH} (Hz)
Flume	0.095	0.006	0.555
Model	0.087	0.007	0.419

Table 4 Normalised velocity profile characteristics for the real vegetation. $\overline{U}$ is the mean shear layer velocity, θ_M is the shear layer momentum thickness and f_{KH} is the predicted Kelvin-Helmholtz frequency using Eq. (8).

	$\overline{U}$ (ms^{-1})	θ_M (m)	f_{KH} (Hz)
Flume	0.207	0.019	0.344
Model	0.207	0.030	0.221

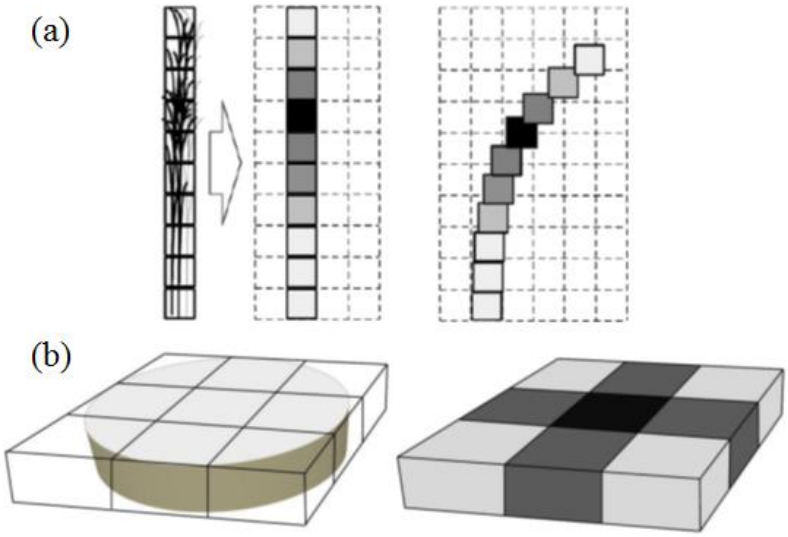

Figure 1 Model schematic showing (a) Tandem plant and LES grid systems (reproduced from Ikeda *et al.* (2001)) where a stalk is conceptualised as a vertical array which then moves and maps onto the LES grid; and (b) the porosity cut-cell treatment (right) of original vegetation stalk (left). Here darker cells represent lower porosity values. Figure 1(a) reprinted from International Journal of Heat and Fluid Flow, 22, Ikeda, S., Yamada, T., Toda, Y., Numerical study on turbulent flow and honami in and above flexible plant canopy, Copyright (2001), with permission from Elsevier.

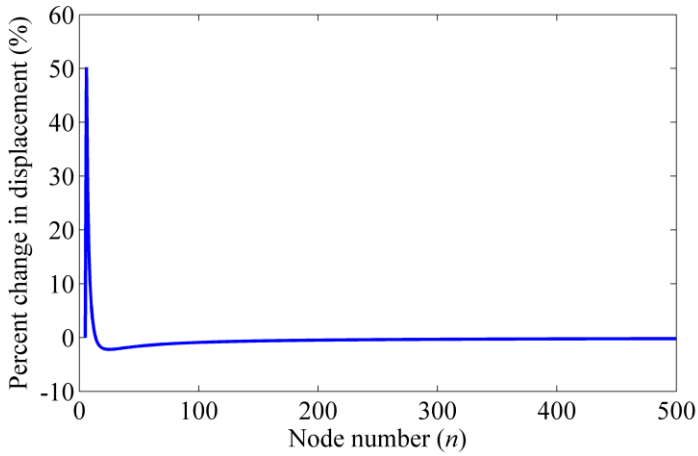

Figure 2 The change in end-node displacement with increasing node number for the Euler-Bernoulli beam model. The change is shown as a percentage of the total displacement.

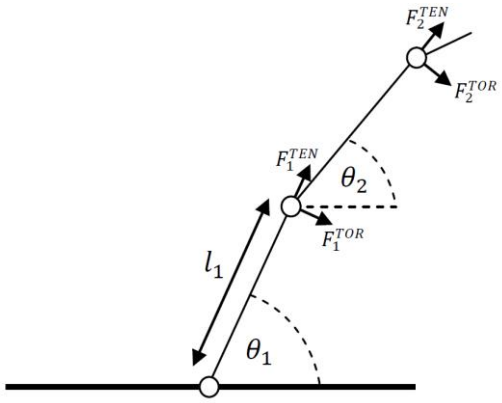

Figure 3 A schematic showing the basis for the N-pendula model. The circles represent model nodes connected by pendula of length l_i each at an angle of θ_i from the horizontal.

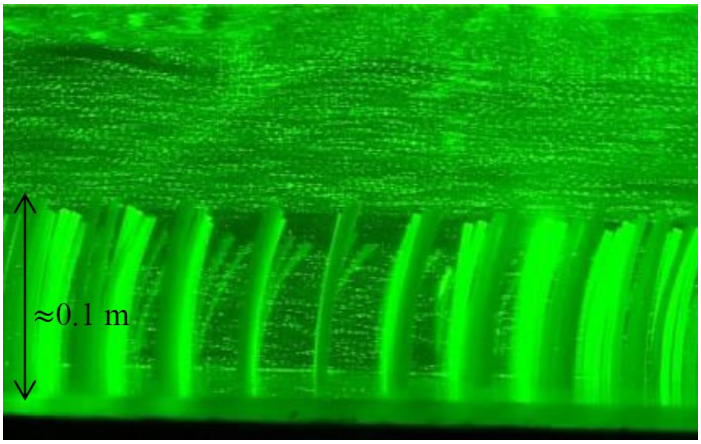

Figure 4 Flexible artificial vegetation used within the flume experiments. Picture taken during the experiments, with flow from left to right.

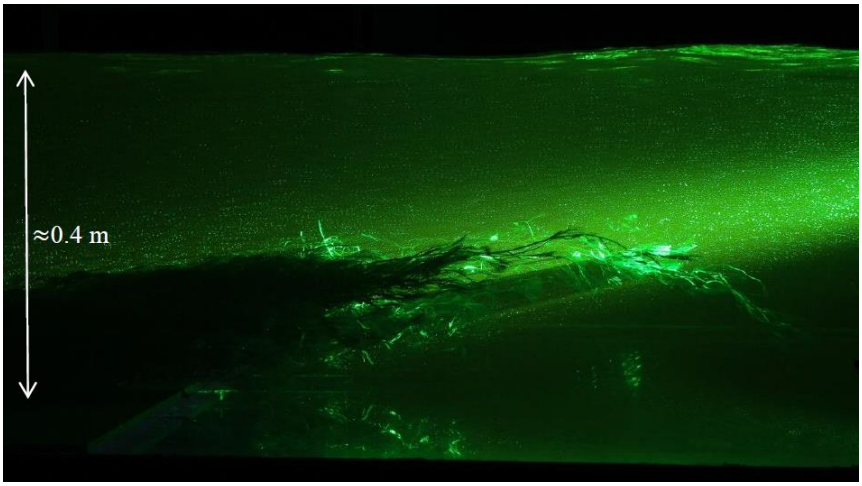

Figure 5 Patches of *Ranunculus penicillatus* fastened to the bed of the flume at the base, for the flume experiments with natural vegetation. Flow is from left to right, with the PIV particles illuminated using a laser positioned downstream of the vegetation.

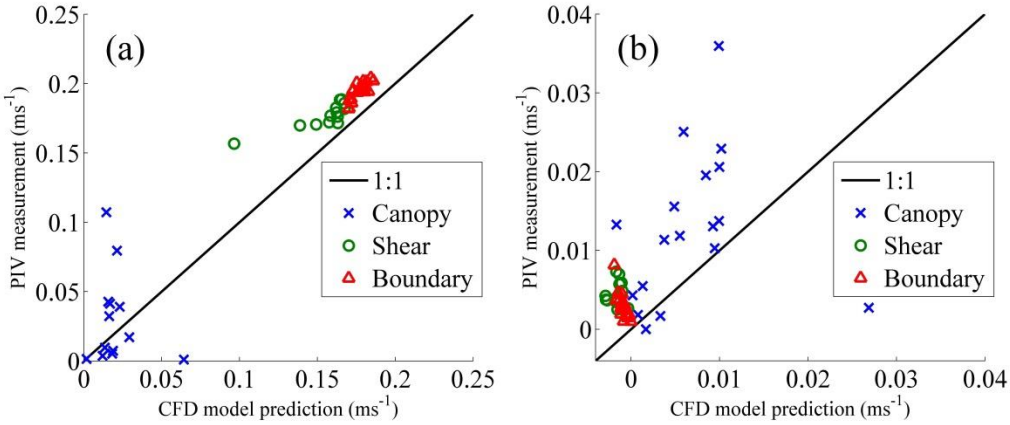

Figure 6 Spot value comparisons for the time-averaged downstream (a) and vertical (b) velocity components. Data points are coloured by region: canopy (blue crosses), shear layer (green circles) and boundary layer (red triangles). The black line indicated a perfect [1:1] relationship.

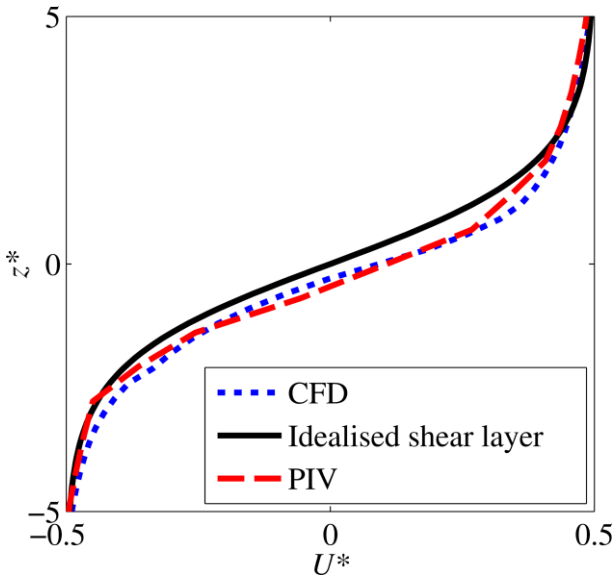

Figure 7 Normalised, time-averaged downstream velocity profiles for the artificial vegetation (PIV) and Euler-Bernoulli beam model (CFD) data. Profiles have also been averaged in the streamwise direction. The black line indicates the idealised hyperbolic tangent shear layer profile.

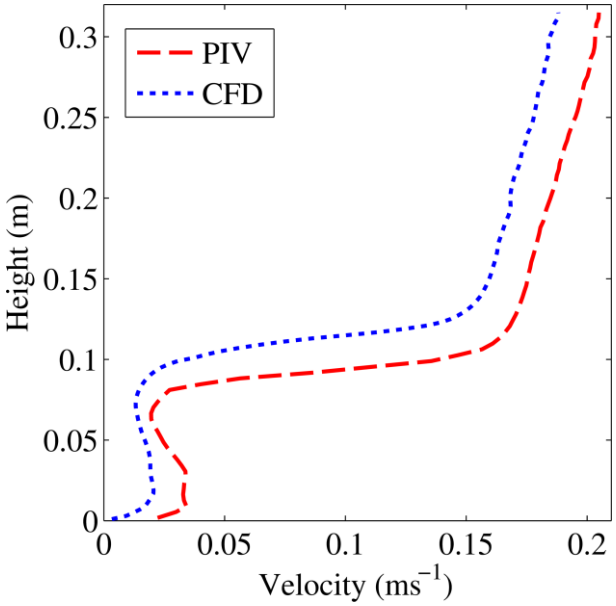

Figure 8 Time-averaged downstream velocity profiles for both the experimental (PIV) and model (CFD) data. Profiles have also been averaged in the streamwise direction.

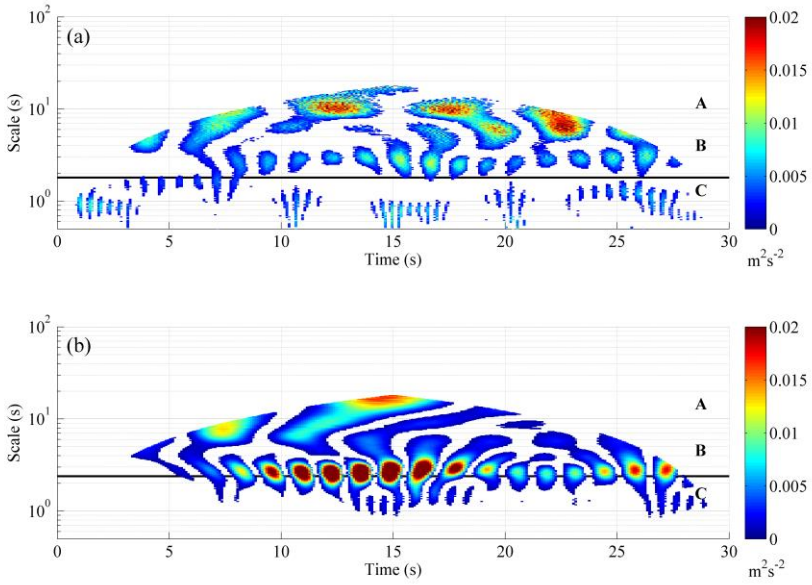

Figure 9 Wavelet spectra for the artificial vegetation (a) and Euler-Bernoulli beam model (b) data. The black lines indicate the estimated Kelvin-Helmholtz frequencies from Table 3.

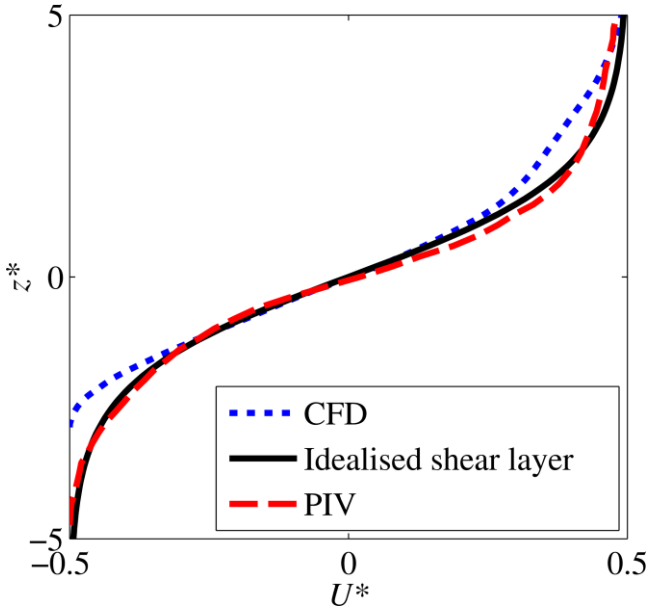

Figure 10 Normalised, time-averaged downstream velocity profiles for the real vegetation (PIV) and N-pendula model (CFD) data. Profiles have also been averaged in the streamwise direction. The black line indicates the idealised hyperbolic tangent shear layer profile.

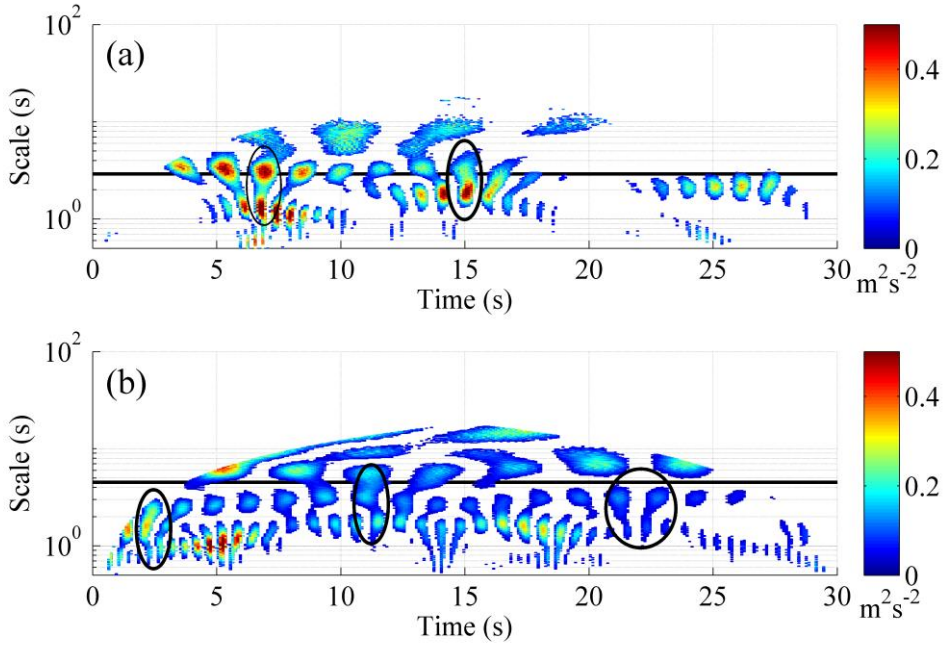

Figure 11 Wavelet spectra for the real vegetation (a) and N-pendula model (b) data. The black lines indicate the estimated Kelvin-Helmholtz vortex frequencies from Table 4. The ovals highlight areas of coalescence.

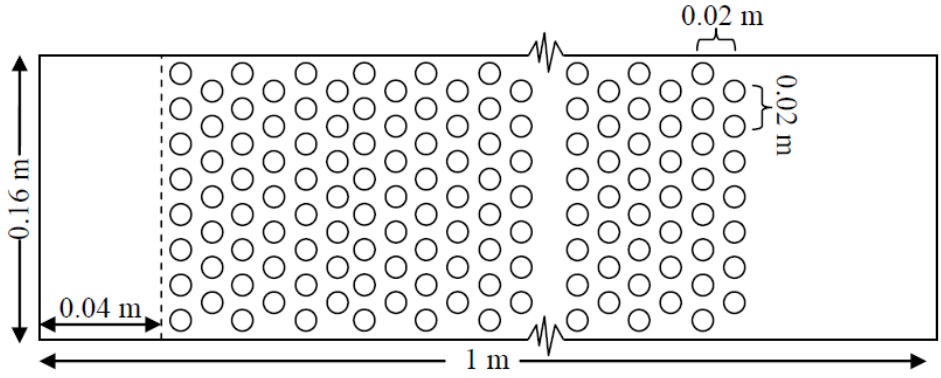

Figure 12 Schematic of the Euler-Bernoulli beam model canopy simulation. The dotted line shows the boundary of the flow recirculation region.

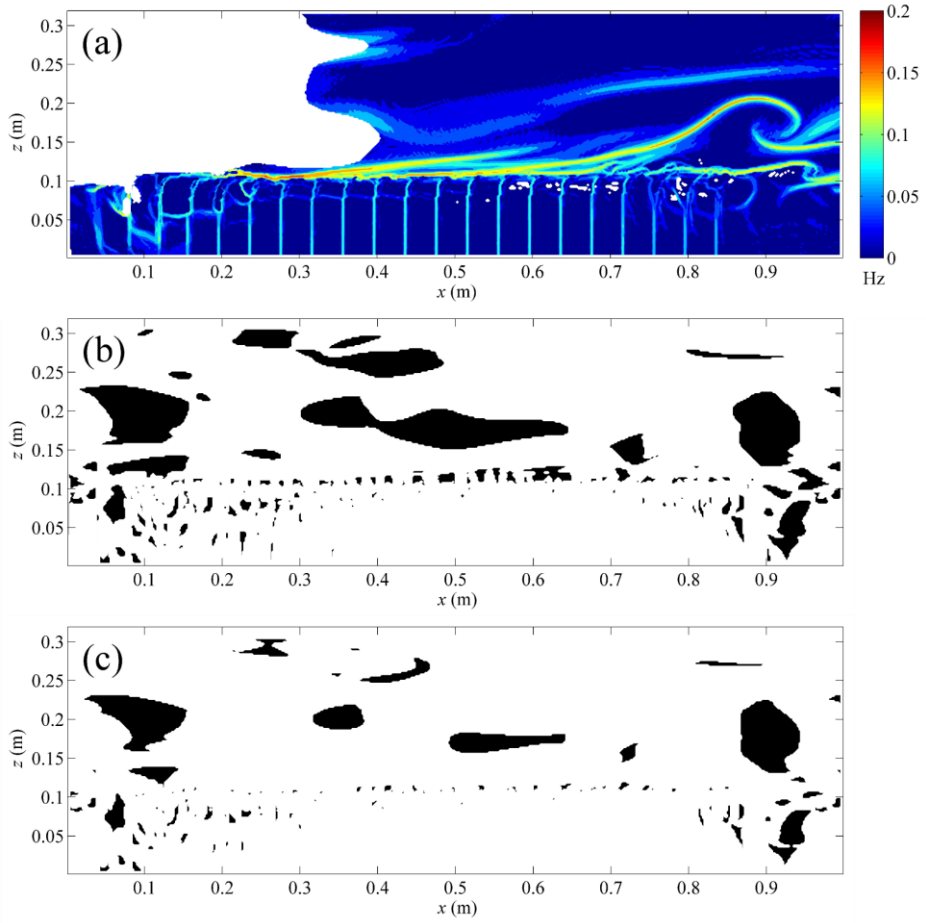

Figure 13 Vortex detection results using the (a) FTLE, (b) Q and (c) λ_2 criterion. In (a), areas in yellow/red represent vortex ridges. In (b) and (c) areas of black represent vortices.

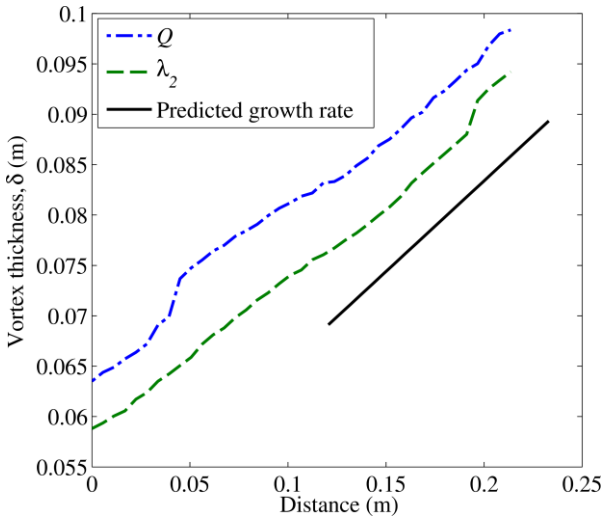

Figure 14 Change in vortex thickness through time using the Q (blue) and λ_2 (green) criteria. The predicted shear layer growth rate is shown in black.

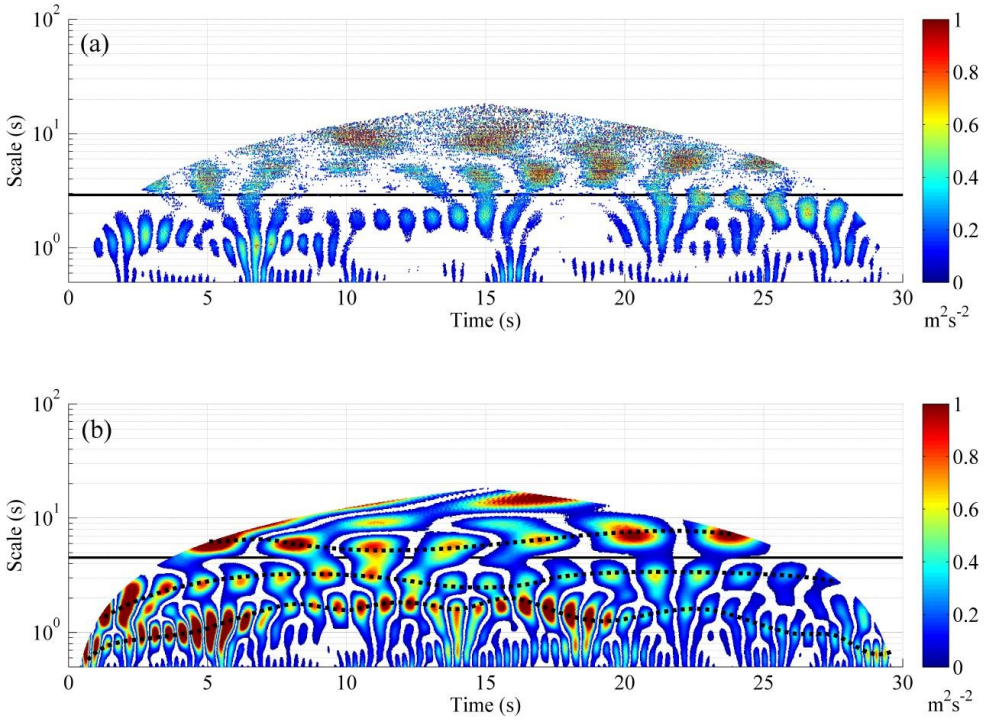

Figure 15 Wavelet spectra for the real vegetation (a) and N-pendula model (b) data at 50 Hz resolution. The black lines represent the estimated Kelvin-Helmholtz frequencies. The dotted black lines highlight varying periodicities through time.